# Particle segregation in turbulent Couette-Poiseuille flow with vanishing wall shear

**By Kun Yang[1], Lihao Zhao[2,1,*] and Helge I. Andersson[1]**

[1]Department of Energy and Process Engineering, Norwegian University of Science and Technology, 7491 Trondheim, Norway

[2]Department of Engineering Mechanics, Tsinghua University, 10084, Beijing, China

e-mail: zhaolihao@tsinghua.edu.cn

## Abstract

Inertial particles dispersed in wall-bounded flows in pipes and channels are known to accumulate close to the walls. The segregation ability depends greatly on the inertia-selection effects of the near-wall quasi-coherent turbulent structures, which are formed near both walls where shear stresses are high. Here, however, we investigated if and how particles segregate in the vicinity of walls in absence of mean shear. A tailor-made turbulent Couette-Poiseuille flow was designed such that the mean shear vanished at the moving wall, thereby resulting in an asymmetric flow with conventional near-wall turbulent structures only at one wall. In addition, Large-Scale Structures (LSSs) were observed in the flow, which greatly influenced the distribution of the inertial particles. Particles of five different inertia groups were embedded in the directly simulated turbulence field and examined. It was found that particles of high inertia segregated near the stationary wall where mean shear prevailed, but also near the moving wall where mean shear was absent. However, due to the qualitatively distinct near-wall flow structures, the inertia effects on the actual segregation were different at the two walls. Mechanisms causing the asymmetric wall-normal segregation were explored with the focus on the moving-wall region, where the quasi-coherent turbulent structures were absent, and the local fluid structures were dominated by imprints of the LSSs.

**Key words:** particle-laden flow, turbulent Couette-Poiseuille flow, inertial particle distribution, Large-Scale Structures

## 1. Introduction

Particle-laden turbulent flows are prevalent in many industrial applications and environmental processes. Examples include dispersion of carbonaceous dust or chemicals, the huge amount of plankton species in the ocean, transport of pollutants in the air, and natural processes such as formation of clouds and rain in the atmosphere and sediment transport in rivers. The dynamics of inertial particles in turbulence and their interactions with the containing fluid have received continuous consideration in various flow configurations in the past decades. However, the commonly encountered flow scenarios are still far from being fully covered and particle mixing in inhomogeneous and anisotropic turbulence remains a largely open question.

Among various scenarios, dispersion of small inertial particles in a pressure-driven turbulent plane channel flow (also known as a turbulent Poiseuille flow) is widely documented. The governing equation for the motion of spherical solid particles in non-uniform flows was first proposed by Maxey and Riley (1983) under the condition that the Reynolds number based on the radius of the sphere is smaller than unity. Based on this theoretical model, McLaughlin (1989) was the first to use Direct Numerical

Simulation (DNS) coupled with Lagrangian particle tracking to study aerosol particle deposition in a turbulent Poiseuille flow (referred to as P flow henceforth) at low Reynolds number.

It has been extensively reported that initially randomly-distributed particles in a turbulent P flow will accumulate in the near-wall region, in particular in the viscous sublayer, under the effects of inertia. This phenomena is often referred to as "turbophoresis", a term literally meaning particle transport operated by turbulence, which was firstly proposed by Caporaloni et al. (1975) and later developed and refined by Reeks (1983, 2005, 2014). There have been several influencing factors that lead to a final segregation. Brooke et al. (1994) separated the particle flux into three groups according to their origin, namely the free-flight flux, the turbophoretic flux and the diffusive flux. They found that the near-wall accumulation resulted mainly from free-flights that do not enable particles to bounce back from the wall, while aided by turbophoresis.

Particle segregation is determined by the coupling between particle inertia and the surrounding fluid structures. Particle inertia is often measured by a non-dimensional parameter, namely the Stokes number (*St*), defined as the ratio of the particle response time ($\tau_p$) to the timescale of the underlying fluid flow ($\tau_f$). The Stokes number reflects the time the particles need to adjust their motions following the variation of the local fluid. The Stokes number for a P flow is often defined using wall units, i.e. $St = \tau_p/\tau_f$ where $\tau_f = \nu/u_\tau^2$ and $\nu$ is the kinematic viscosity of the fluid and $u_\tau$ is the friction velocity at the wall. Previous studies have demonstrated that the strongest near-wall segregation follows a non-monotonic trend with *St*. For example, for a P flow with $Re_\tau = 180$ ($Re_\tau$ based on the friction velocity $u_\tau$ and the channel half-height $h$), the strongest near-wall segregation is found at $St \approx 20 \sim 30$, while either decreasing or increasing *St* will lead to a weaker segregation (Marchioli and Soldati 2002; Picciotto et al. 2005; Soldati and Marchioli 2009). The *St*-dependency of near-wall deposition is evaluated by Narayanan et al. (2003), who proposed three different regimes: the Brownian diffusion (for $St < 0.2$), the diffusion-impaction regime ($0.2 < St < 20$) and the inertia-moderated regime ($St > 20$).

The carrying flow undertakes inertia-selection of the particles. The quasi-coherent streaky structures and the associated elongated streamwise vortices are the most prominent structural features of wall-bounded flows in the inner layer ($z^+ < 60$) (Jeong et al. 1997; Schoppa and Hussain 2002). When particles are added into the turbulence, the combined effects of the near-wall quasi-coherent turbulent structures together with particle inertia determine the final segregation in the viscous sublayer (Kaftori et al. 1995a,b; Rouson and Eaton 2001; Marchioli and Soldati 2002, 2009). In particular, Marchioli and Soldati (2002) provided a detailed description of the mechanism for the optimal *St* for maximum near-wall segregation. They pointed out the important inertia-selection effects of the offspring streamwise vortices inhabiting the particles to leave the wall. The ability to successfully escape the wall region depends on the particle inertia, or *St*. Tracer-like particles follow the flow perfectly and obey the fluid continuity, whereas particles of large-inertia (e.g. $St = 100$) with strong wall-ward momentum hit the wall and bounce back into the outer flow while ignoring the offspring streamwise vortices. Particles with intermediate inertia (e.g. $St \approx 30$) have the strongest segregation inside the viscous sublayer, because for them inhabitation of offspring vortices is most effective. While the effects of the near-wall structures are obviously significant, it is however worthwhile mentioning that some studies have demonstrated accumulation of particles in low-turbulence regions in flows without near-wall quasi-coherent structures, see e.g. Iliopoulos et al. (2003), Skartlien (2007), Arcen and Tanière (2009), indicating that the near-wall turbulent structures may not be the direct cause of near-wall segregation.

Most studies on particle dispersion in wall-bounded flows have focused on the near-wall quasi-coherent turbulent structures, and very few paid attention to the influences of the Large-Scale Structures (LSSs) in the core region commonly encountered in some flows (Bernardini et al. 2013). For example, LSSs are observed in pipe and channel flows at high $Re_\tau$ (Kim and Adrian 1999), but DNSs of particle-laden turbulent P flows at high $Re_\tau$ are still impracticable due to extensive computational cost (the highest $Re_\tau$ ever reported is $Re_\tau = 1000$ by Bernardini 2014). However LSSs can be observed in a turbulent Couette flow (C flow) even at low or moderate $Re_\tau$, which thus serves as a good background flow to evaluate the effects of LSSs on particle dispersion. In a C flow the two walls have a relative velocity which drives the in-between fluid. Turbulent C flows have coexisting turbulent streaks near the walls and the LSSs in the core region which interact with each other non-linearly (Kitoh et al. 2005; Bech et al. 1995). Although these interactions have crucial effects on particle dispersion, relevant studies are rare (Bernardini et al. 2013; Richter and Sullivan 2013, 2014). One example to mention here is Bernardini et al. (2013), who conducted DNS coupled with Lagrangian particle tracking for a C flow at $Re_\tau = 167$ and compared with a P flow at $Re_\tau = 183$. They found the highest near-wall segregation at $St = 25$ for both the C flow and the P flow. Streamwise particle streaks were observed in the near-wall region for both flows, but the characteristic patterns of the streaks were essentially different, as a result of imprinting of the outer-layer LSSs onto the inner-layer fluid structures. While the C flow is a good choice for evaluating particle distribution under the influences of LSSs, the existence of near-wall structures makes it difficult to isolate the effects of LSSs in the near-wall region.

A combined turbulent C and P flow, namely the turbulent Couette-Poiseuille flow (CP flow), is a more computationally affordable prototype for evaluating the LSSs in wall-bounded flows (Kuroda et al. 1995; Pirozzoli et al. 2011; Yang et al. 2017). Compared to a C flow, the CP flow requires a smaller domain than that needed for a C flow (Bech et al. 1995; Tsukahara et al. 2006), since the LSSs generated in the core region is shorter in streamwise direction than those formed in a C flow (Pirozzoli et al. 2011). The CP flow has two controlling parameters, i.e. both a streamwise pressure gradient and a relative wall motion. In particular, with a carefully chosen combination of the controlling parameters, the mean shear and thus the turbulent regeneration events can be eliminated at one wall (Pirozzoli et al. 2011; Coleman et al. 2017; Yang et al. 2017). Due to the distinguishing near-wall structures at the opposing walls and also the presence of LSSs in the core region, the zero-mean-shear CP flow is a useful flow vehicle to explore individually the influences of both the near-wall streaks and the LSSs on particle distribution in turbulence. The CP flow is of theoretical importance, for example, it was used by Thurlow and Klewicki (2000) to understand the mechanisms of drag reduction in ultra-hydrophobic surfaces, and by Coleman et al. (2017) to improve turbulence closure models. In practice, the CP flow resembles the flow beneath a ship operating at small underkeel clearance (Gourlay 2006).

It is worthwhile to point out a flow similar to the zero-mean-shear CP flow, i.e. the open-channel or free-surface flow. Studies on open-channel flows (Pan and Banerjee 1995; van Haarlem et al. 1998; Narayanan et al. 2003; Nagaosa and Handler 2003; Righetti and Romano 2004) are inspiring for studies on the current CP flow due to some similarities in these two flows at first sight: both flows have asymmetric flow structures near the two opposing walls, and the near-wall quasi-coherent turbulent structures are observed only near the wall with maximum mean shear while they are absent near the shear-free surface. The asymmetric near-wall flow structures cause variation of the near-wall particle segregations for the two walls in an open-channel flow (van Haarlem et al. 1998; Narayanan et al. 2003). However, the boundary conditions at the shear-free surface are different in these two flows (no-slip for CP flow and free-slip for open-channel flow). Thus the wall-normal distributions of the turbulence intensities and the r.m.s. vorticity are distinctly different near this wall (Nagaosa and Handler 2003; Yang et al. 2017). More importantly, the large scales observed in the two flows are essentially different. In an open-channel flow, the large-scale upwellings and downwellings in the bulk of flow are caused by the large-scale near-wall sweeps and ejections imprinting from near the no-slip wall to the free-slip wall. On the contrary, in the current CP flow sweep and ejection events are relatively small-scale and confined near the stationary wall like in a P flow. The longitudal LSSs that we observe in a CP flow at low $Re_\tau$ are large-scale streamwise circulations which are not present in an open-channel flow at a similar $Re_\tau$.

It is our prime interest to investigate wall-normal particle segregation under the effects of the surrounding fluid (particularly the LSSs) and particle inertia. A specific turbulent CP flow with zero mean wall shear at the moving wall is considered, which enables us to investigate the influences of the LSSs on near-wall particle behaviors without the influence of near-wall turbulent structures. The outline of the paper is as follows. After presenting our methodology, some crucial features of the CP flow are firstly presented, before giving a complete description of the particle deposition in this particular flow. The distinguishing wall conditions of the particular CP flow result in an asymmetric segregation at two walls. By evaluating this observation, mechanisms of particle wall-normal segregation is proposed and further understood.

## 2. Methodology

This paper presents a DNS study coupled with Lagrangian particle tracking of a particle-laden turbulent CP flow with zero mean shear at one wall. A sketch of the computational domain is shown in Figure 1, where a Newtonian fluid is driven by a streamwise pressure gradient between two parallel plates in relative motion separated by a distance of 2*h*. The flow is governed by the incompressible Navier-Stokes equation and the continuity equation. The Reynolds number considered here is $Re_{\tau,S}$ = 180, based on the friction velocity at the stationary wall ($u_{\tau,S}$), half channel-height ($h$) and kinematic viscosity $v$.

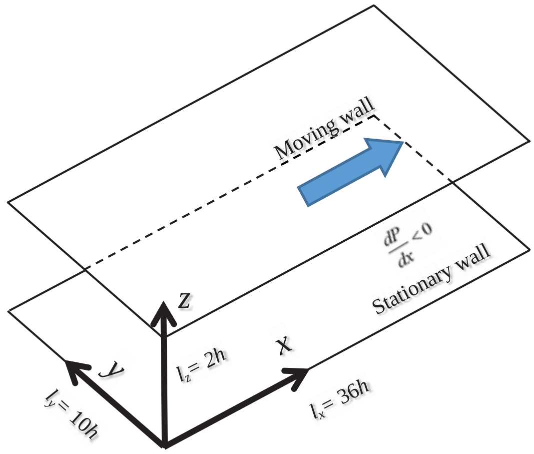


Figure 1. Sketch of the present computational domain.

We use an Eulerian approach for the fluid phase. As shown in Figure 1, a Cartesian coordinate system $\vec{x} = (x, y, z)$ is applied, and the size of the whole domain is $l_x$ (streamwise) × $l_y$ (spanwise) × $l_z$ (wall-normal) = 36*h* × 10*h* × 2*h*. In the homogenous directions ($x$ and $y$), periodic boundary conditions are applied. The two parallel walls are assumed infinitely long and wide, and are both impermeable and applied with a no-slip boundary condition. The bottom wall ($z/h$ = 0) is set to be stationary while the top wall ($z/h$ = 2) has a relative velocity of $U_{\text{wall}} = 20u_{\tau,S}$. This velocity was chosen together with the streamwise-driving pressure gradient to achieve a vanishing mean shear at the moving wall. For the present CP flow, we obtained a statistically negligibly low total mean shear of $|T^{+}| \approx 3\times10^{-3}$ at the moving wall. In this paper, unless otherwise stated, all quantities with superscript + are normalized using viscous units, by $u_{\tau,S}$ for velocity, $v/u_{\tau,S}$ for length and $v/u^2_{\tau,S}$ for time. For domain discretization, the number of grid points is 576 × 260 × 192 in the $x \times y \times z$ directions, respectively. The grid size in the homogeneous $xy$-plane is uniform, with $\Delta x^{+} \times \Delta y^{+} = 11.25 \times 6.93$. In the wall-normal direction, the grids are non-uniform, and are symmetric about the channel center plane with increasingly finer size closer to the walls. The first grid near the wall has the smallest grid spacing with $\Delta z^{+}$ = 0.88 and the largest grid spacing ($\Delta z^{+}$ = 2.86) is placed at the channel center. More details regarding the validity of the present domain size and mesh resolution were discussed in Yang et al. (2017), which provides an established database of the current CP flow. The flow was calculated using a pseudo-spectral method in the homogeneous directions, and a second-order central finite-difference method in the wall-normal direction. The pressure field is obtained by solving a Poisson equation using FFT in the homogenous directions and a tri-diagonal matrix algorithm in the wall-normal direction. An explicit second-order Adams-Bashforth scheme is used for time advancement, with a time step of $\Delta t = 0.0002h/u_{\tau,S}$, or $\Delta t^{+}$ =

0.036. The DNS code has been used and validated in various previous studies (Gillissen et al. 2007; Mortensen et al. 2008; Zhao et al. 2010, 2012, 2013; Yang et al. 2017).

Particles were added into the fully-developed statistically-steady turbulent CP flow at random locations and tracked at each time step (same as for the Eulerian fluid) in a Lagrangian framework. The present study considers rigid and point-like (i.e. particles with diameter $d_p/h = 2\times10^{-3}$ are smaller than Kolmogorov microscale) spherical particles with varying inertia. We consider only a dilute suspension where particle-particle collisions and feedback of particles on the fluid can be neglected. In the present work the particles are only subject to the Stokes drag force while all other forces, e.g. lift and gravity, are neglected. The position of each particle is determined by a Lagrangian point-particle tracking approach which is the same as that adopted by Mortensen et al. (2008) and Zhao et al. (2010, 2012, 2013). The initial particle velocity was prescribed to equal the local Lagrangian fluid velocity, which was obtained by using a quadratic interpolation scheme applying information from the 27 closest grid-points (van Haarlem 2000). The position and velocity of each particle is updated by integration of the following equations forward in time:

$$\frac{d\vec{x}_{\mathrm{p}}}{dt} = \vec{u}_{\mathrm{p}} \qquad \text{and} \qquad \frac{d\vec{u}_{\mathrm{p}}}{dt} = \frac{1}{\tau_{\mathrm{p}}}\left(\vec{u}_{\mathrm{fp}} - \vec{u}_{\mathrm{p}}\right)\left(1 + 0.15\,\mathrm{Re}_{\mathrm{p}}^{0.687}\right), \tag{2.1}$$

where $\vec{x}_{\mathrm{p}} = (x_{\mathrm{p}}, y_{\mathrm{p}}, z_{\mathrm{p}})$ is the particle position, and $\tau_{\mathrm{p}} = 2Da^2/9\nu$ is the particle response time with $D = \rho_{\mathrm{P}}/\rho$ being the density ratio of the particles to the carrier fluid. In particular, $\vec{u}_{\mathrm{fp}}$ is the instantaneous Lagrangian fluid velocity vector at the particle position, $\vec{u}_{\mathrm{fp}} = (\tilde{u}_{\mathrm{fp}}, \tilde{v}_{\mathrm{fp}}, \tilde{w}_{\mathrm{fp}})$ in $x$, $y$ and $z$ directions respectively, to be distinguished with the fluid velocity vector at the Eulerian grid points, $\vec{u}_{\mathrm{f}} = (\tilde{u}_{\mathrm{f}}, \tilde{v}_{\mathrm{f}}, \tilde{w}_{\mathrm{f}})$; and $\vec{u}_{\mathrm{p}}$ is the instantaneous particle velocity vector, $\vec{u}_{\mathrm{p}} = (\tilde{u}_{\mathrm{p}}, \tilde{v}_{\mathrm{p}}, \tilde{w}_{\mathrm{p}})$. By means of a Reynolds-decomposition, $\tilde{u} = U + u$, $\tilde{v} = V + v$ and $\tilde{w} = W + w$, where $U$, $V$ and $W$ are mean velocity components, and $u$, $v$ and $w$ are the corresponding velocity fluctuations. The last term in Eq. (2.1) is a semi-empirical correction which extends the validity of the drag force equation (Schiller and Naumann 1933). Periodic boundary conditions are imposed in the homogeneous directions. For particle-wall collisions, a perfect elastic reflection condition is applied at both walls, when the distance between the particle center and the wall is smaller than the particle radius $a$.

As mentioned in the Introduction, particle inertia is measured by a non-dimensional Stokes number, defined as $St = \tau_{\mathrm{p}}/\tau_{\mathrm{f}}$. Note that $St$ based on the viscous units is a global parameter, i.e. it is not a function of particle location. In this study, five different particle groups are considered with $St = 0.2$, 1, 5, 30 and 100, respectively. For each $St$ group, a total number of 2.5 million particles were introduced in the computational domain and remained throughout the calculation, with no particles removed.

# 3. Results

## 3.1. *Turbulent CP flow properties*

The mean streamwise velocity $U$ in the CP flow with vanishing wall shear increases monotonically all the way from the stationary wall at $z = 0$ to the moving wall at $z = 2h$. The statistically steady state of the flow field is reflected by the spatio-temporal averaged stresses shown in Figure 2 (a). The distribution of the total mean shear stress (normalized by viscous units) $T^+ = dU_f^+/dz^+ - \overline{u_f^+ w_f^+}$ of a statistically stationary turbulent CP flow with zero mean shear at $z^+ = 2h^+$ should follow a linear relation $T = -\left(dP/dx\right)\left(2h - z\right)$, or $T^+ = 1 - z^+/2h^+$, obtained from integration of the x-component of the Reynolds-averaged Navier-Stokes equation in the wall-normal direction (Tennekes and Lumley 1972). The linearity of $T^+$ is clearly observed in Figure 2. The maximum values occur at (for mean viscous shear stress and mean total stress) or near (for Reynolds stress) the stationary wall, while all mean stresses vanish at $z^+ = 2h^+$ ($z/h = 2$). To be more exact, at the moving wall a statistically low mean value of $|T^+| \approx 3\times10^{-3}$ is obtained in the present study. This turbulent CP flow field is discussed in greater details in Yang et al. (2017).

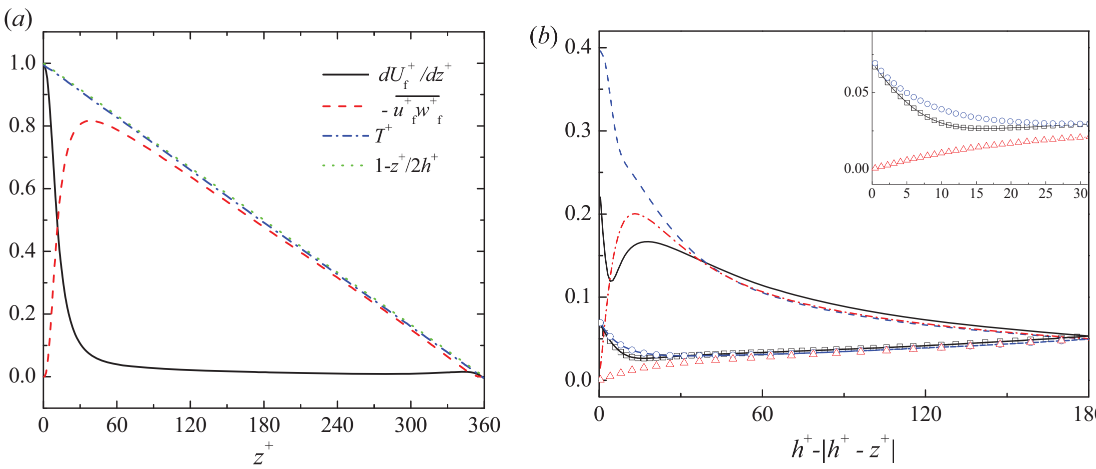


Figure 2. Statistical fluid properties normalized by wall units. (a) Wall-normal distribution of shear stresses, where $1 - z^+/2h^+$ is the reference straight line obtained from the Reynolds-averaging. (b) Comparison of normalized vorticity fluctuations near the two walls, where the horizontal axis shows the distance away from the nearby wall. The lines are for near the stationary wall: —— $\omega^+_{x,rms}$; - - - $\omega^+_{y,rms}$; and -·-· $\omega^+_{z,rms}$. The lines with symbols are for near the moving wall: black solid line with squares: $\omega^+_{x,rms}$; blue dash line with circles: $\omega^+_{y,rms}$; and red dash-dot line with triangles: $\omega^+_{z,rms}$. The subplot shows the quantities zoomed in near the moving wall region.

The most relevant flow structures for our discussion in this paper are the small-scale quasi-coherent turbulent structures near the stationary wall and the global LSSs (Yang et al. 2017). To demonstrate these two different scales, firstly the wall-normal distribution of the normalized components of the fluctuating vorticity vector are shown in Figure 2 (b) where $\omega^+_{x,rms}$, $\omega^+_{y,rms}$ and $\omega^+_{z,rms}$ are in streamwise, spanwise and wall-normal directions, respectively. As can be observed, the vortical structures at the two walls are clearly distinctive. Next to the stationary wall (denoted by lines), quasi-coherent streamwise vortices cause a peak of $\omega^+_{x,rms}$ at $z^+ \approx 20$. On the contrary, in the moving wall region (denoted by lines with symbols), all vorticity components have low values with no near-wall peaks, except for a small increase leading to a modest maximum value at the wall caused by the impermeability of the no-slip wall (Kim et al. 1987), indicating the absence of quasi-coherent structures as those formed near the stationary wall.

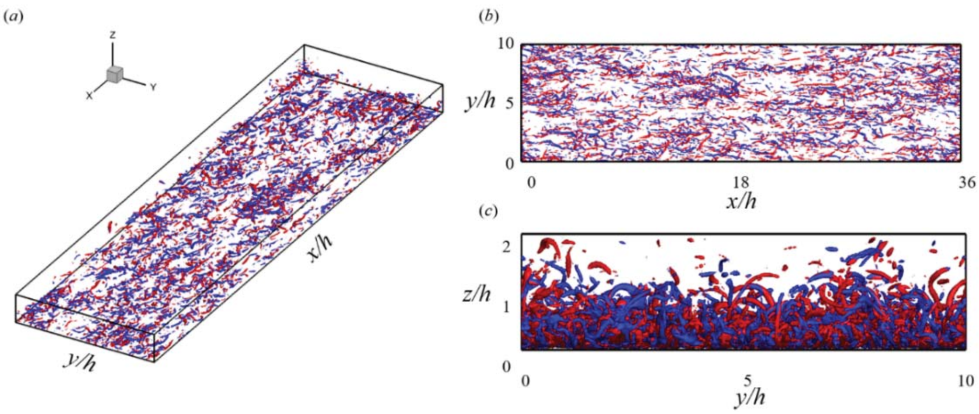


Figure 3. Instantaneous iso-surfaces of $\lambda_2 = -0.05$ for the instantaneous flow field, with view of the whole domain (a), from the top (b) and from the front (c). Colours on the iso-surfaces are associated with the sign of streamwise vorticity ($\omega_x$).

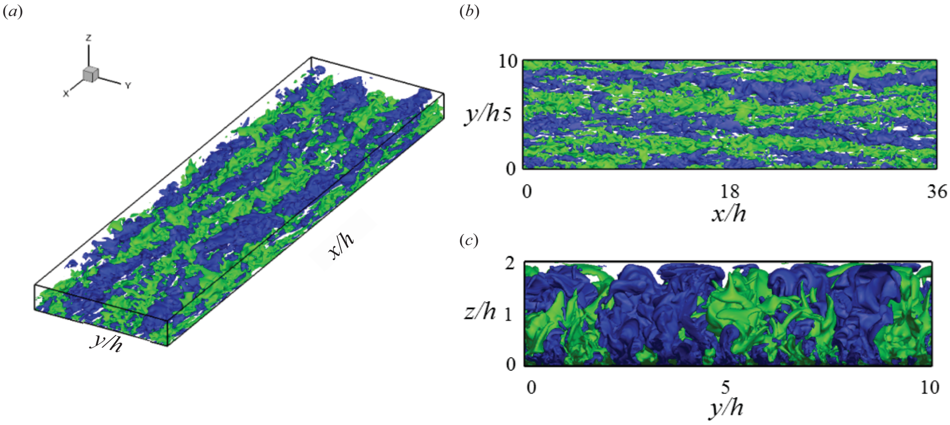


Figure 4. Normalized instantaneous iso-surfaces of $u^+_f/u^+_{f,rms}$ = 1.5 (green) and -1.5 (blue) for the instantaneous flow field, with view of the whole domain (a), from the top (b) and from the front (c).

The LSSs are visualized in Figure 4 via iso-surface of the normalized streamwise velocity fluctuations ($u^+_f/u^+_{f,rms}$) for the instantaneous flow field. It is seen that the LSSs are much more elongated in the streamwise direction than the small-scale near-wall streaks. In the wall-normal direction, the LSSs spread throughout the channel and extend their influences into the near-wall quasi-coherent structures, causing an increase of spanwise spacing of the quasi-coherent near-wall streaks in the buffer layer (Yang et al. 2017). The quasi-coherent LSSs in the core region induce persistent wall-normal flows and play an important role in the overall momentum exchange, by linking the flow field near the two walls (Bernardini et al. 2013). Therefore, although the LSSs are much weaker in strength compared to the small-scale quasi-coherent near-wall structures (Figure 2 (b) and Figure 3), the LSSs are expected to have a key effect on the particle distribution, as shall be discussed later.

To demonstrate the characteristics of the local fluid structures in the CP flow with the presence of LSSs, the wall-normal profile of the normalized Kolmogorov microscales of the present CP flow is compared with a P flow in Figure 5. Near the stationary wall, the values of the normalized Kolmogorov length scale $\eta_K^+$ and time scale $\tau_K^+$ are very similar in the two cases. Away from the stationary wall, $\eta_K^+$ and $\tau_K^+$ increase for both flows, but near the core region, values of $\eta^+_{K,\mathrm{P}}$ and $\tau^+_{K,\mathrm{P}}$ become larger than those of $\eta^+_{K,\mathrm{CP}}$ and $\tau^+_{K,\mathrm{CP}}$, indicating that the dissipation in the center occurs at larger microscale structures for the P flow than for the CP flow. Beyond the center plane and toward the moving wall, $\eta^+_{K,\mathrm{P}}$ and $\tau^+_{K,\mathrm{P}}$ decrease due to the symmetry of the P flow field, while $\eta^+_{K,\mathrm{CP}}$ and $\tau^+_{K,\mathrm{CP}}$ continue to increase. The length scale $\eta^+_{K,\mathrm{CP}}$ reaches a maximum of 5 and the time scale $\tau^+_{K,\mathrm{CP}}$ a maximum of over 20 very close to the moving wall, followed by a sharp drop for both $\eta^+_{K,\mathrm{CP}}$ and $\tau^+_{K,\mathrm{CP}}$. The monotonic increase of $\eta^+_{K,\mathrm{CP}}$ and $\tau^+_{K,\mathrm{CP}}$ across the core region results from the gradually reducing mean shear, and the sudden decrease next to the moving wall is attributed to the proximity of a solid wall. The enlargement of the Kolmogorov microscales near the moving wall compared to the stationary wall is essential in understanding the particle distributions in this area.

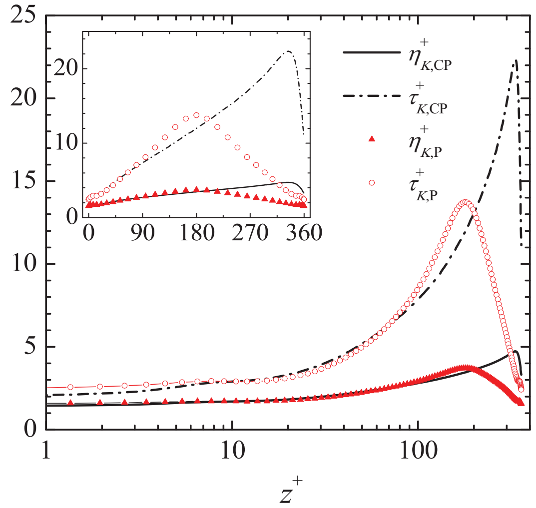


Figure 5. Wall-normal distribution of the normalized Kolmogorov microscales for length $\eta_K$ and time $\tau_K$ compared to P flow by Kim et al. (1987). Large plot in semi-log scale and inner plot in linear scale.

## 3.2. *Particle distribution in the CP flow*

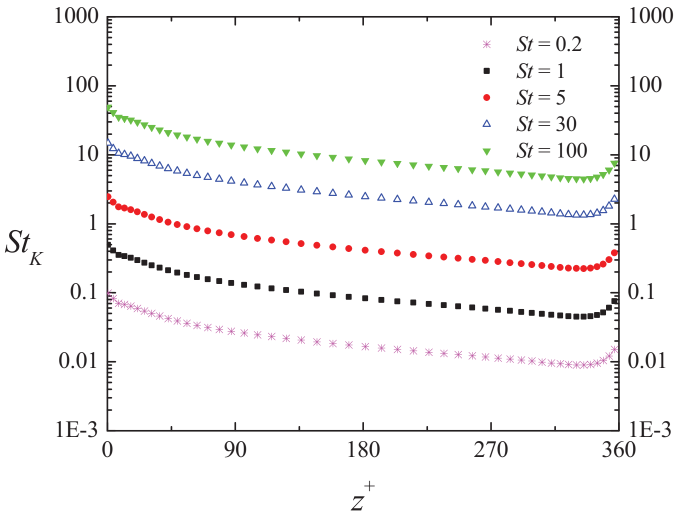


Figure 6. Local $St_K$ based on local Kolmogorov time microscale $\tau_K$ versus global $St$ based on viscous time scale $\tau_f$.

In the present study we will evaluate five particle groups of Stokes number $St = 0.2$, 1, 5, 30 and 100 defined based on the viscous time scale $\tau_f$. As seen in Figure 5, the local fluid micro-scales vary greatly from the stationary wall to the moving wall, and it is therefore reasonable also to define a local Stokes number based on the local Kolmogorov microscale $\tau_K$ as $St_K = \tau_p/\tau_K$, just as in homogenous isotropic turbulence (HIT). As observed by Picano et al. (2010) for particle-laden jet flows, a local Stokes number can be crucial in determining particle transport. The relation between the local $St_K$ and the global $St$ is then $St_K = St/\tau_K^+$, which is plotted in Figure 6. fWhile $St$ is a global parameter, $St_K$ varies with the local microscale and is associated with the local fluid structures. Figure 6 shows that the local $St_K$ decreases for each $St$ from the stationary wall to the moving wall, as a result of increasing $\tau^+_{K,CP}$ (Figure 5). The value of the local $St_K$ at the moving wall for each global $St$ incidentally matches the value of $St_K$ at the stationary wall for a smaller $St$, e.g. $St_K$ for $St = 30$ at the moving wall $\approx St_K$ for $St =$ 5 at the stationary wall (see also Figure 9 (b)). It is particularly noteworthy that $St_K$ is close to unity near the moving wall for $St = 30$ particles. In this paper we categorize the particles according to the global $St$, but will explain some observations in terms of the local $St_K$.

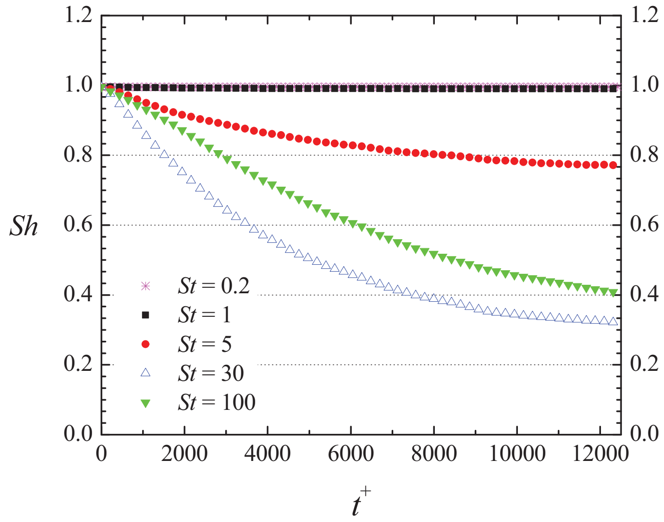


Figure 7. Evolution of the global Shannon entropy calculated over the whole domain for different particle groups. Note that the data for $St$ = 0.2 and 1 are overlapping at $Sh \approx 1$ .

After the particles were initially introduced at random locations in the fully developed turbulent CP flow, they slowly accumulate near the walls due to so-called “turbophoresis”. A global parameter, namely the normalized Shannon entropy, can be used to quantify the overall time and spatial evolution of particle distribution in the whole channel (Picano et al. 2009 and Bernardini 2014). In order to measure particle mixing, the whole domain was divided into $N_{\mathrm{bin}}$ = 200 uniformly distributed wall-parallel bins. The global Shannon entropy is defined as $Sh(t) = H(t)\,/\max(H(t))$, where $H(t) = -\sum_{k=1}^{N_{bin}} p(k,t)\ln p(k,t)$ with $p(k,t)$ the possibility of finding a particle in the $k^{\mathrm{th}}$ bin at time $t$, $p(k) = NP(k,t)/NP_{\mathrm{total}}$, and $\max(H) = \ln N_{\mathrm{bin}}$. Here $NP(k, t)$ is the number of particles in the $k^{\mathrm{th}}$ bin at time $t$, and $NP_{\mathrm{total}}$ is the total number of particles in the whole domain ($NP_{\mathrm{total}} = 2.5\times10^6$ for each particle group). Following its definition, the normalized Shannon entropy reveals the degree of global wall-normal inhomogeneity. A uniform dispersion will result in $Sh$ = 1, while the most concentrated case (i.e. if all particles are segregated in a single bin) leads to $Sh$ = 0. Figure 7 shows the evolution of $Sh$ for different $St$ values. $Sh$ for all cases starts at 1 as particles of all groups were initially injected into the flow field at random locations, and remains so for particles of low inertia ($St$ = 0.2 and 1) which maintain a random distribution throughout the simulation. A monotonic decrease of $Sh$ is seen for $St$ = 5, 30 and 100, indicating the wall-normal segregation of inertial particles into different bins. The group of $St$ = 30 is the fastest to form the most segregated particle field (reflected by the lowest $Sh$); the degree of wall-normal homogeneity of the particle field decreases more slowly for $St$ = 5 and 100, and reaches a less concentrated particle distribution compared to $St$ = 30 (reflected by a higher $Sh$). The simulation ran up to over 12000 viscous time units (in total $3.5\times10^5$ time steps). As can be seen in Figure 7, almost all curves approach asymptotically to constant $Sh$-values, except $St$ =100 for which the particles respond most slowly to the fluid and need the longest time to reach segregation equilibrium. The simulations were terminated here because i) the present samplings fulfil our primary aim of study, which is to qualitatively and quantitatively evaluate the distribution of particles with different inertia values in this CP flow, and ii) continuing the simulation will unnecessarily cost extensive computing resources and time without adding further information. The same reasoning was made by Marchioli et al. (2008).

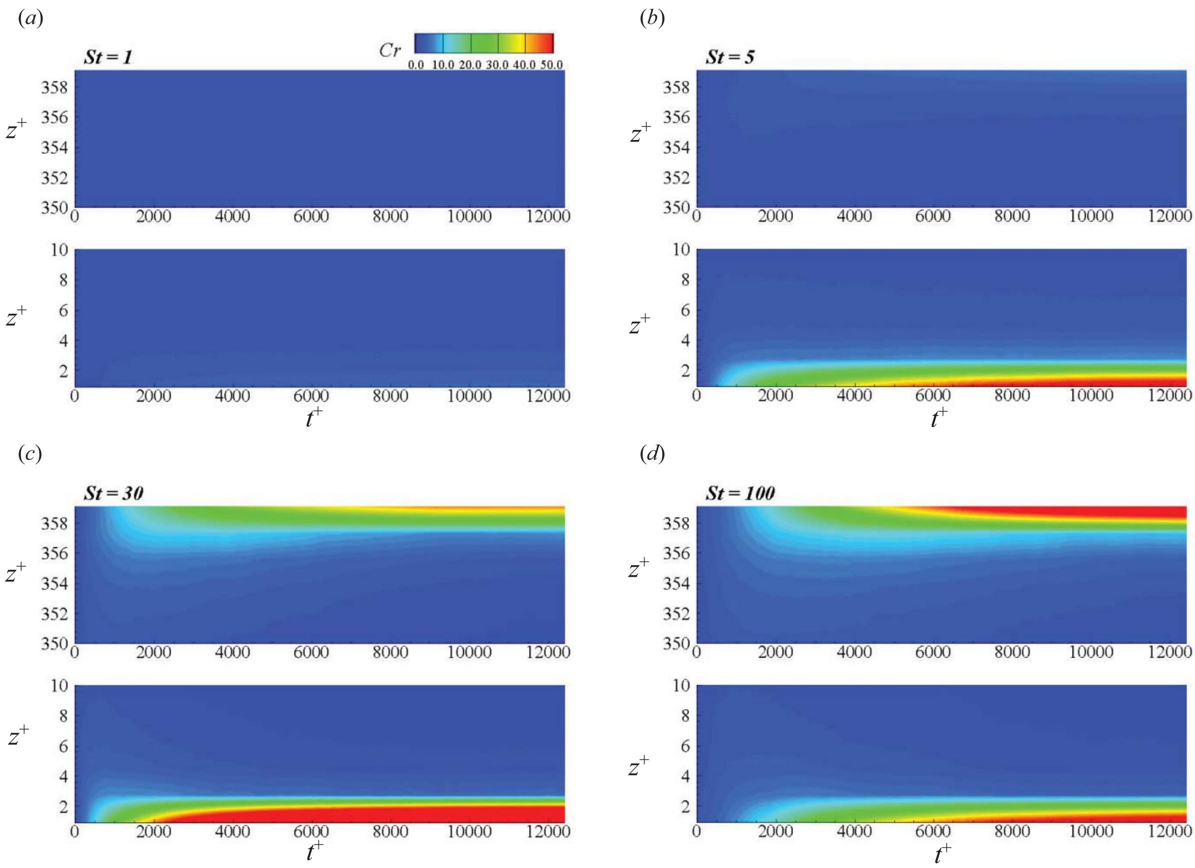


Figure 8. Spatio-temporal evolution of particle wall-normal concentration *Cr* for (a) $St = 1$, (b) $St = 5$, (c) $St = 30$, and (d) $St = 100$ in the near-wall region. For each case, the lower plot shows the stationary wall region from $z^+ = 0$ to 10 and the upper plot shows the moving wall region from $z^+ = 350$ to 360. The contour levels of *Cr* are from 0 to 50.

To reveal the temporal development of local particle segregation, in particular near the walls, a concentration parameter is defined as $Cr(k, t) = NP(k,t)/NP(k,0)$. Following this definition, $Cr > 1$ indicates particle accumulation and $Cr < 1$ indicates particle depletion in the $k^{\text{th}}$ bin at time $t$. The evolution of particle segregation in the near wall region is demonstrated via spatio-temporal contours of *Cr* in Figure 8 for *St* = 1, 5, 30 and 100, respectively. Note that the case of $St = 0.2$ in this type of plot appears very similar to the case of $St = 1$, and is thus not shown for brevity. Effects of *St* on the particle segregation process are clearly observed in Figure 8. As time advances, tracer-like particles of $St \lesssim 1$ remain almost randomly dispersed throughout the simulation, while particles of $St \geq 5$ begin to accumulate in thin layers near the walls. The latest inception of near-wall segregation is observed for the heaviest particles of $St = 100$. The distribution of *Cr* near the two walls is distinctly asymmetric. In particular, particles of *St* = 5 and 30 obviously have a much stronger tendency to accumulate near the stationary wall, while for $St = 100$ particle accumulation seems to be similar near both walls.

Near-wall particle segregation for different *St* values is quantitatively presented in the instantaneous wall-normal distribution of *Cr* in Figure 9 (a). Dense near-wall accumulation is observed for highly inertial particles, which results in depletion of particles in the core region (inner plot of Figure 9 (a)) and leads to a constant $Cr < 1$ throughout a large range of the domain. Near the stationary wall, it is not surprising to see that the *St*-dependency of particle segregation bears similarities with a P flow, considering similar flow structures in this region in the two flows (Marchioli and Soldati 2002; Zhao et al. 2010). The near-wall accumulation for inertial particles shows a non-monotonic *St*-dependency, i.e. strongest segregation observed for $St = 30$ and followed by $St = 100$, 5, 1 and 0.2 in a decreasing-segregation order. For *St* = 30 and 100, *Cr* decreases to below 1 just outside the viscous sublayer, indicating particle depletion from the buffer layer. However for smaller $St$ ($St \leq 5$), a thicker segregation layer (above the viscous sublayer and into the buffer layer) is observed. In general the particles accumulate in a very thin layer next to the stationary wall, below the near-wall quasi-coherent structures at about at $z^+ \approx 12$ in the buffer layer.

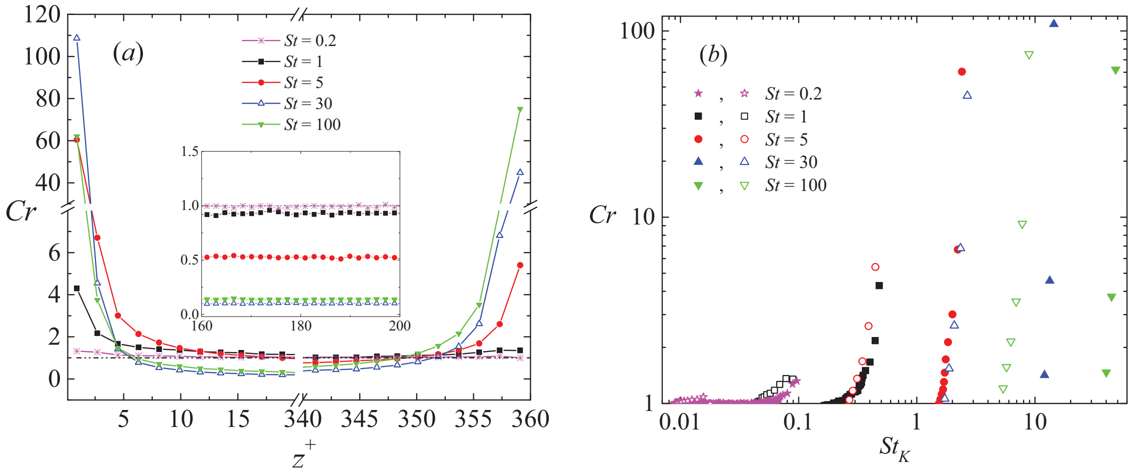


Figure 9. Instantaneous concentration ($Cr$) (a) profile near the walls and in the center region (sub-plot) and (b) distribution versus local $St_K$. Both at $t^+ = 12420$. For clarity, in (a) the horizontal axis is broken between $z^+ = 20$ and 340, and vertical axis between $Cr = 8$ and 30. The dash-dot line stands for $Cr = 1$, i.e. the demarcation value between particle accumulation ($Cr > 1$) and particle depletion ($Cr < 1$). In (b) solid symbols represent near the stationary wall and open symbols near the moving wall.

The particle segregation is clearly not symmetric with respect to the channel centerline, and several differences of $St$-dependency of $Cr$ are found near the moving wall. Compared to the stationary wall, the degree of accumulation is lower for $St \leq 30$, and higher only for $St = 100$. Near the moving wall the $St$-dependency of $Cr$ exhibits a monotonic drop with the decreasing of particle inertia. In addition, the accumulation layer is thicker compared to the stationary wall. These phenomena are attributed to the different effects of LSSs near the moving wall and the near-wall turbulent structures near the stationary wall, as shall be explained later. It is interesting to note from Figure 9(a) that each of the $Cr$ profiles near the moving wall seem to resemble one of a lower $St$ near the stationary wall, e.g. $St = 30$ (moving wall) is comparable to $St = 5$ (stationary wall), etc. This similarity can be associated with the local Stokes number $St_K$ corresponding to the time scale of the local fluid structures formed under different mean shear conditions, as mentioned before in conjunction with Figure 6. To demonstrate this point more clearly, $Cr$ as a function of $St_K$ based on the local Kolmogorov timescale is shown in Figure 9(b). It is observed that although $St$ is different, a similar near-wall $St_K$ results in similar $Cr$, regardless of the amount of mean shear.

An explanation of the particle near-wall segregation described above is now proposed with the focus on the region near the moving wall. Particle segregation results from the combined effects of the surrounding fluid and the particle inertia. Considering the absence of the sweep and ejection events near the moving wall, the LSSs and the corresponding wall-induced vorticity are thus crucial for entraining the particles to move toward and away from the wall. To check the correlation between the persisting LSSs and the particle segregation, Figure 10 hows the spatio-temporal averaged flow field and the contours of $Cr$, as well as the particle wall-normal velocity ($w^+_p$) contours in the cross-flow plane for the sample case of $St = 30$. The spatial averaging was performed in the streamwise direction, and the temporal averaging was performed over 10 large-eddy turnover times, defined as $\tau_L = 2h/u_{\tau,S}$. Depending on the circulation direction of the LSSs (shown by the streamlines), large amount of fluid is pushed either towards or away from the nearby wall in the region where two counter-rotating large-scale vortices meet (red arrows). Such regions are correlated with either a trough or crest of particle segregation area (shown by contours of $Cr$ in Figure 10 (a)). Near the moving wall, a more distinct and larger segregation area is observed where two large-scale vortices meet and generate a downward wash (red arrows pointing away from the wall), and a smaller segregation area is observed with an upward wash (red arrows pointing towards the wall). The influence of the LSSs on particle accumulation is much more obvious near the moving wall than near the stationary wall with quasi- coherent streamwise vortices. In addition, Figure 10 (b) shows that the bulky LSSs group the overall wall-normal translation of particles by oppositely signed $w^+_p$, and the upward fluid parcel is clearly correlated with particles going towards the moving wall ($w^+_p > 0$ in red) while the downward fluid parcel with $w^+_p < 0$ (blue). Also, $w^+_p$ is larger in the channel center and goes to zero at the wall, as shall be mentioned again later.

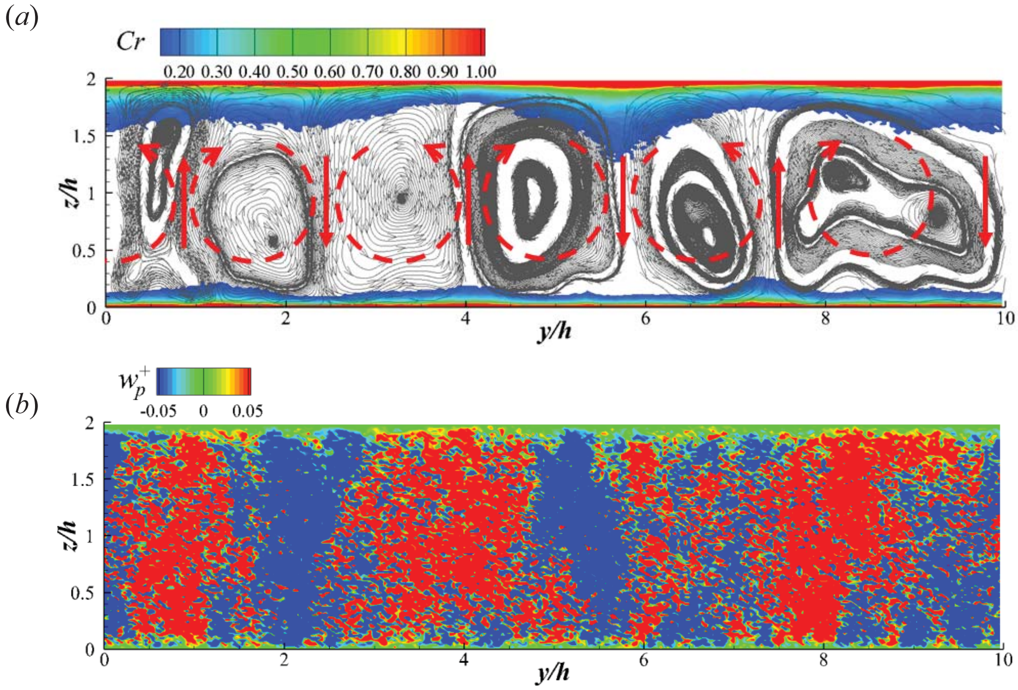


Figure 10. Correlation between wall-normal particle translation and the long-persisting LSSs. (a) Spatio-temporal averaged contours of $Cr$ (showing particle accumulation) for particles of $St = 30$, and the LSSs visualized by streamlines. Contour level shown for $0.15 \leq Cr \leq 1$. Conceptual sketch of the LSSs is shown by red circles, and the vertical red arrows pointing in the flow direction of the combined wall-normal wash by neighboring LSSs. (b) Spatio-temporal averaged contours of wall-normal particle velocity $w^+_p$. Particles moving towards the stationary wall (i.e. negative $w^+_p$) are indicated by blue and those towards the moving wall (i.e. positive $w^+_p$) by red. Both (a) and (b) are averaged over 10 large-eddy turnover times and along the streamwise direction.

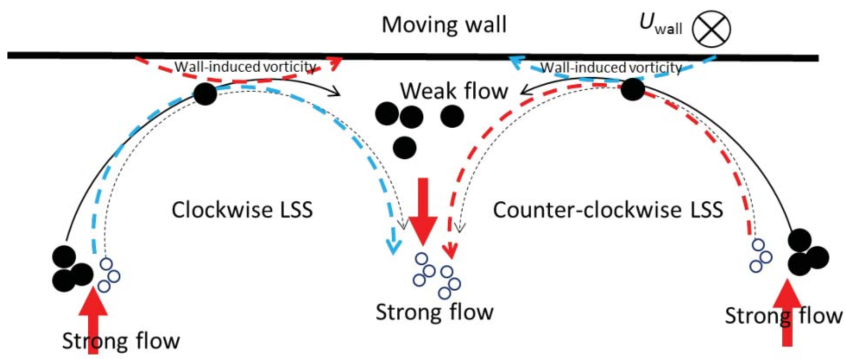


Figure 11. Sketch of particle segregation near the moving wall under the combined effects of the LSSs and particle inertia. Large solid circles represent particles of large inertia and small empty circles represent particles of small inertia. The turbulent intensity is strong in the channel center (denoted as

"strong flow") and weak near the wall (denoted as "weak flow"), see Yang et al. (2017). Solid red arrows point in the direction of wall-normal flow wash by the neighboring LSSs. Particles of large inertia stay in near-wall weak flow region while particles of small inertia follow the flow to leave the near-wall region.

In addition to LSSs, particle inertia determines how the particle will react to the carrying fluid. The mechanism of *St*-dependency of particle segregation in the region with near-wall turbulent structures was discussed by Marchioli and Soldati (2002), as mentioned in the Introduction. For the current CP flow, a sketch to explain the mechanism near the moving wall is given in Figure 11. It has been shown in Figure 10 that the LSSs play an important role in wall-ward particle translation, especially near the moving wall without the strong near-wall turbulent structures. Once a particle reaches the moving wall, it can leave the wall region through (1) wall-rebouncing and/or (2) entrainment by off-wall flow advection. To check the importance of (1), the average frequency of particle-wall collisions is presented in Table 1. First, comparing between the two walls, a reduced possibility of collisions near the moving wall is observed for all *St*, indicating less importance of particle-wall collisions in this region. The reduced collision frequency is due to the absence of strong near-wall sweeps. Second, with the increasing of *St*, the collision frequency first increases, reaches a maximum, and then drops. This trend is seen at both walls, but the *St* value which gives the highest collision frequency is different at the two walls, and is also different from *St* that gives the highest segregation (*Cr*) for each wall. The two differences result from the inertia-selection effects from the offspring streamwise vortices which are only present near the stationary wall (Marchioli and Soldati 2002). In particular, the highest collision rate is found for particles comparable to the local fluid scale, i.e. $St_K \approx 1$, which corresponds to $St = 5$ at the stationary wall and $St = 30$ at the moving wall (Figure 6). For our current discussion, suffice it to say with observations from Table 1 that particle-wall collision is playing a very limited role in particle segregation near the moving wall. Considering particle movements associated with particle-wall collisions, few particles with large inertia hit the wall and bounce back with high off-wall velocity. This is because i) mechanical energy is obtained from the weak LSSs alone and ii) there is no assistance from strong sweep and ejections. Even the small population that does collide with the moving wall will bounce back with low off-wall velocity, which is insufficient for them to travel far away from the moving wall.

Table 1. Averaged frequency (number per viscous time unit) of particle-wall collision at each wall. $NC_S$ is the average frequency of collisions at the stationary wall and $NC_M$ is the average frequency of collisions at the moving wall.

| ***St*** | **0.2** | **1** | **5** | **30** | **100** |
|---|---|---|---|---|---|
| $\boldsymbol{NC_S}$ | 16 | 25 | 57 | 21 | 10 |
| $\boldsymbol{NC_M}$ | 0 | 0 | 13 | 17 | 4 |

Effects of particle re-entrainment by the local fluid (point (2)) are discussed with reference to Figure 11. Recall that the vorticity magnitude of the LSSs is very small (Figure 2 (b)). Therefore once high-inertia particles from the center reach the near-wall region where the local turbulence advection is very low, the off-wall rotation from the weak LSSs is unable to change the direction of $w^+_p$ and to carry the particles to leave the near-wall region and back into the core region. As a result, high-inertia particles tend to end up to have low velocity and to segregate in the low-advection region near the moving wall. To confirm this reasoning, Figure 12 shows the p.d.f. of the particle wall-normal velocity and the wall-normal Lagrangian fluid velocity at the particle location. As seen in Figure 12 (a), particles accumulate in off-wall ($w^+_{fp} < 0$) fluid advection regions where the fluid velocity magnitude is low. This trend becomes clearer for particles of larger inertia due to the effect of inertia-filtering, i.e. tracers follow the fluid better whereas particles with large inertia filter the fluid flow. From Figure 12 (b) it is seen that most high-inertia particles have very low off-wall velocity, meaning that they are unlikely to move far away from the wall. The larger the particle inertia, the higher particle population with low off-wall velocity, and the more likely to result in a higher segregation in the near-wall region.

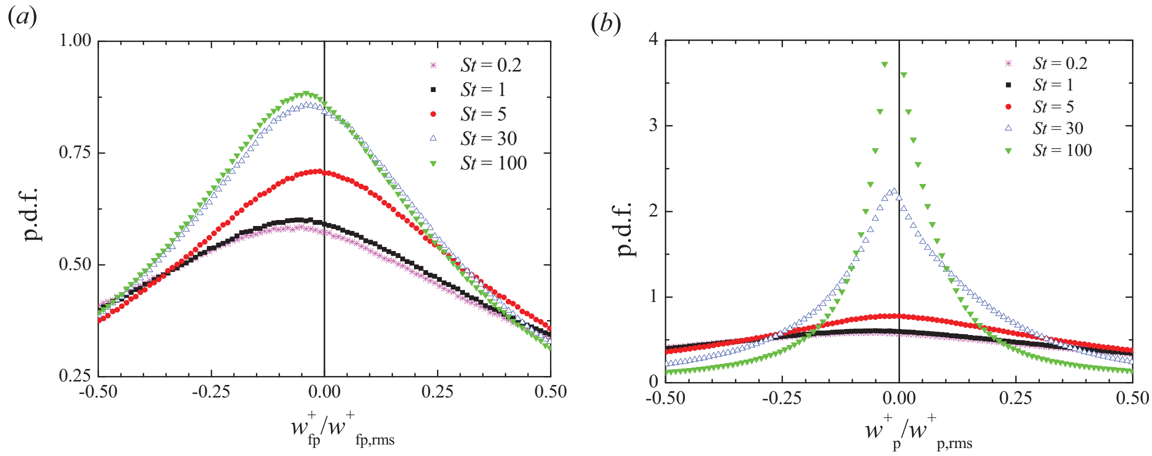


Figure 12. P.d.f. of normalized wall-normal velocity. (a) Lagrangian fluid velocity at particle positions and (b) particle velocity near the moving wall in the range of $z^+$ = 339 ~ 359 ($\Delta z^+$ = 20). The normalization parameter $w^+_{rms}$ is localized in each $\Delta z^+ = 1$. The results are averaged using 60 samples in time.

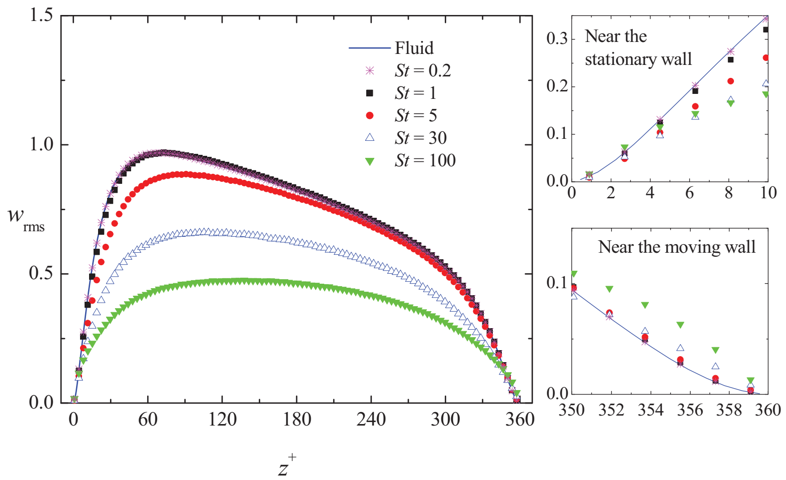


Figure 13. Profile of the normalized wall-normal Eulerian fluid ($w^+_{f,rms}$) and Lagrangian particle ($w^+_{p,rms}$) velocity fluctuation. Note that the fluid profile almost overlaps with $St$ = 0.2 particles.

To further demonstrate the coupling between the particle inertia and the LSSs, which is the reason for causing the observations in Figure 12, a comparison between the fluid and the particle velocity fluctuations is given in Figure 13 across the whole channel. Due to the inertia-filtering mechanism, $w^+_{p,rms}$ for higher $St$ values is lower in the core region, and reduces more slowly approaching the walls. As a result of the strong near-wall turbulent regeneration events near the stationary wall, inertial particles have smaller velocity fluctuations than the flow ($w^+_{p,rms} < w^+_{f,rms}$) due to inertia-filtering with the local strong turbulent events. Near the moving wall, $w^+_{p,rms}$ follows a monotonic decrease by reducing $St$ (similar to the trend of $Cr$). Local advection is confirmed to be relatively low ($w^+_{f,rms} < w^+_{p,rms}$) especially for the particles with large inertia, which are then too inertial to change direction and get re-entrained in the off-wall wash by the weak LSSs. The high-inertia particles will therefore follow their own trajectories and remain close to the wall. The fact that the insufficiency of the LSSs in providing enough off-wall momentum is more severe for particles of larger $St$ can be further interpreted by considering the local Kolmogorov scales (Figure 5). Near the moving wall the local small scales are much larger than near the stationary wall, and can therefore be ignored only by particles of larger *St* and/or with higher off-wall velocity. The larger the particle inertia, the more inadequate the LSSs become, and thus the more particles will accumulate near the moving wall.

The above discussions show that the presence of near-wall quasi-coherent turbulent structures is not a prerequisite to induce near-wall particle segregation. However, their presence clearly changes the actual deposition ability for particles of a certain inertia. Near the stationary wall, the near-wall quasi-coherent turbulent structures are the dominating factor in performing *St*-selection, while near the moving wall the LSSs play an important role in determining the *St*-trend of the near-wall segregation.

# 4. Conclusions

In this paper we discussed segregation of inertial particles in a specific shear-free Couette-Poiseuille flow by means of DNS coupled with Lagrangian particle-tracking. The flow has been designed such that the moving wall eliminates the mean shear and therefore also the near-wall quasi-coherent turbulent structures, and causes the flow field to be asymmetric with respect to the channel centre. The two distinct wall regions in the present CP-flow facilitate a direct evaluation of the effects of different near-wall turbulent structures on the behaviour of inertial particles. Near the stationary wall, quasi-coherent turbulent streaks are formed, which are similar to those observed in a turbulent Poiseuille flow (P flow). These streaks are strong, but local and modestly persistent in time and space. An important feature of the present zero-shear CP flow is the formation of Large-Scale Structures (LSSs). These structures are weak, but are almost global and more persistent than the conventional near-wall streaks. More details of the un-laden CP flow can be found in Yang et al. (2017).

The asymmetric flow field leads to asymmetric particle segregation behaviour which varies from wall to wall. In this study five groups of inertial particles were evaluated, which were denoted as $St$ = 0.2, 1, 5, 30 and 100. The non-monotonic *St*-dependency of the particle segregation (*Cr*) near the stationary wall is similar to that found in the canonical P flow (Marchioli and Soldati 2002). However, *Cr* follows a monotonic drop with decreasing *St* near the moving wall. Considering the variation of *Cr* for each *St* between the two walls, except for particles of $St$ = 100 that have an increased segregation near the moving wall, particles of all other (lower) *St* values show a weaker segregation near the moving wall than near the stationary wall. In addition, particles tend to accumulate in a thicker wall-normal layer near the moving wall.

Mechanisms for the variation of particle wall-normal segregation from wall to wall are explored and proposed in the present study with the focus on the moving-wall region. Near-wall segregation results from coupling between the local fluid and the particle inertia. The global LSSs in the current CP flow are found to play a crucial role in the overall particle mixing (Figure 10), especially next to the moving wall where no quasi-coherent turbulent structures are formed. In this region, particles moving toward and away from the wall are determined by the LSSs alone, which play a crucial role in inertia-selection (compared with the crucial role played by the strong near-wall turbulent structures at the opposite wall). Two mechanisms responsible for wall-ward and off-wall particle translation in the moving-wall region are the particle-wall collision and the off-wall flow advection. We found that the importance of particle-wall collision decreases greatly near the moving wall compared to the stationary wall, and plays a limited role in reducing the particle number in this region. This is because the weak LSSs alone, without the help of the strong near-wall sweeps, are unlikely to supply sufficient kinetic energy for a large number of high-inertia particles to hit the wall and/or bounce back into the outer flow with high off-wall velocity. Considering the local off-wall fluid advection, it is also quite weak (since the LSSs are weak) in absence of the local strong ejections, and is insufficient to re-entrain particles with large inertia and carry them back into the core region. In addition, the local flow structures are enlarged by the vanishing mean shear near the moving wall, which means that inertia-filtering (i.e. the ability to ignore the local structures) is more effective for larger particles here compared to near the stationary wall. To conclude, the LSSs become less efficient in particle re-entrainment for the higher-inertia particles, for which a stronger segregation near the moving wall results (monotonically decreasing *St*-trend of *Cr*).

The tailor-made CP flow has served as an appropriate vehicle in which particle dispersion can be explored in a qualitatively and quantitatively different turbulence field than the frequently studied near-wall turbulence in boundary layers and channels. We could therefore conclude that inertial particles may segregate in the vicinity of a solid wall, depending on the particle inertia, even in the absence of mean shear. In other words, the presence of the strong quasi-coherent turbulent structures is not a prerequisite for near-wall particle segregation. However, the *St*-effect on the actual segregation ability will be greatly altered from the wall region where quasi-coherent turbulent structures form.

## Acknowledgement

The authors would like to thank The Research Council of Norway (NFR) for providing financial support for the current study through research Grant No. 250744. Our thanks go to Sigma2 for their support in computational resources through Grant No. NN2649K. Finally, we wish to acknowledge the anonymous reviewers for useful comments and suggestions on the revision of this paper.

## References

Arcen, B., Tanière, A., 2009. Simulation of a particle-laden turbulent channel flow using an improved stochastic Lagrangian model. Phys. Fluids 21, 043303.

Bech, K., Tillmark, N., Alfredsson, P.H., Andersson, H.I., 1995. An investigation of turbulent plane Couette flow. J. Fluid Mech. 286, 291–325.

Bernardini, M., Pirozzoli, S., Orlandi, P., 2013. The effect of large-scale turbulent structures on particle dispersion in wall-bounded flows. Intl J. Multiphase Flow 51, 55–64.

Bernardini, M., 2014. Reynolds number scaling of inertial particle statistics in turbulent channel flows. J. Fluid Mech. 758, R1.

Brooke, J.W., Hanratty, T.J., McLaughlin, J.B., 1994. Free-flight mixing and deposition of aerosols. Phys. Fluids 6, 3404.

Caporaloni, M., Tampieri, F, Trombetti, F., Vittori, O., 1975. Transfer of particles in nonisotropic air turbulence. J. Atmos. Sci. 32, 565–568.

Coleman, G.N., Pirozzoli, S., Quadrio, M., Spalart, P., 2017. Direct numerical simulation and theory of a wall-bounded flow with zero skin friction. Flow Turbul. Combust. In press.

Gillissen, J.J.J., Boersma, B.J., Mortensen, P.H., Andersson, H.I., 2007. On the performance of the moment approximation for the numerical computation of fiber stress in turbulent channel flow. Phys. Fluids 19, 035102.

Gourlay, T., 2006. Flow beneath a ship at small underkeel clearance. J. Ship Res. 50, 250–258.

van Haarlem, B., Boersma, B.J., Nieuwstadt, F.T.M., 1998. Direct numerical simulation of particle deposition onto a free-slip and no-slip surface. Phys. Fluids 10, 2608.

van Haarlem, B., 2000. The dynamics of particles and droplets in atmospheric turbulence. PhD Thesis. Delft University of Technology.

Iliopoulos, I., Mito, Y., Hanratty, T.J., 2003. A stochastic model for solid particle dispersion in a nonhomogeneous turbulent field. Intl J. Multiphase Flow 29, 375–394.

Jeong, J., Hussain, F., 1995. On the identification of a vortex. J. Fluid Mech. 285, 69–94.

Jeong, J., Hussain, F., Schoppa, W., Kim, J., 1997. Coherent structures near the wall in a turbulent channel flow. J. Fluid Mech. 332, 185–214.

Kaftori, D., Hetsroni, G., Banerjee, S., 1995a. Particle behavior in the turbulent boundary layer. I. Motion, deposition, and entrainment. Phys. Fluids 7, 1095–1106.

Kaftori, D., Hetsroni, G., Banerjee, S., 1995b. Particle behavior in the turbulent boundary layer. II. Velocity and distribution profiles. Phys. Fluids 7, 1107–1121.

Kim, J., Moin, P., Moser, R., 1987. Turbulence statistics in fully developed channel flow at low Reynolds number. J. Fluid Mech. 177, 133–166.

Kim, K.C., Adrian, R. J., 1999. Very large-scale motion in the outer layer. Phys. Fluids 11, 417–422.

Kitoh, O., Nakabyashi, K., Nishimura, F., 2005. Experimental study on mean velocity and turbulence characteristics of plane Couette flow: low-Reynolds-number effects and large longitudinal vortical structure. J. Fluid Mech. 539, 199–227.

Kuroda, A., Kasagi, N., Hirata, M., 1995. Direct numerical simulation of turbulent plane Couette-Poiseuille flows: effect of mean shear rate on the near-wall turbulence structures. Turbulent Shear Flows 9: Selected Papers from the Ninth International Symposium on Turbulent Shear Flows. Springer, Berlin, Heidelberg. 241–257.

Marchioli, C., Soldati, A., 2002. Mechanisms for particle transfer and segregation in a turbulent boundary layer. J. Fluid Mech. 468, 283–315.

Marchioli, C., Soldati, A., Kuerten, J.G.M., Arcen, B., Tanière, A., Goldensoph, G., Squires, K. D., Cargnelutti, M.F, Portela, L.M., 2008. Statistics of particle dispersion in direct numerical simulations of wall-bounded turbulence: Results of an international collaborative benchmark test. Intl J. Multiphase Flow 34, 879–893.

Maxey, M.R., Riley, J. J., 1983. Equation of motion for a small rigid sphere in a nonuniform flow. Phys. Fluids 26, 883–889.

McLaughlin, J.B., 1989. Aerosol particle deposition in numerically simulated channel flow. Phys. Fluids 1, 1211–1224.

Mortensen, P.H., Andersson, H.I., Gillissen, J.J.J., Boersma, B.J., 2008. Dynamics of prolate ellipsoidal particles in a turbulent channel flow. Phys. Fluids 20, 093302.

Nagaosa, R., Handler, R.A., 2003. Statistical analysis of coherent vortices near a free surface in a fully developed turbulence. Phys. Fluids 15, 375–394.

Narayanan, C., Lakehal, D., Botto, L., Soldati, A., 2003. Mechanisms of particle deposition in a fully developed turbulent open channel flow. Phys. Fluids 15, 763–775.

Pan, Y., Banerjee, S., 1995. A numerical study of free-surface turbulence in channel flow. Phys. Fluids 7, 1649–1664.

Picano, F., Sardina, G., Casciola, C.M., 2009. Spatial development of particle-laden turbulent pipe flow. Phys. Fluids 21, 093305.

Picano, F., Sardina, G., Gualtieri, P., Casciola, C.M., 2010. Anomalous memory effects on transport of inertial particles in turbulent jets. Phys. Fluids 22, 051705.

Picciotto, M., Marchioli, C., Soldati, A., 2005. Characterization of near-wall accumulation regions for inertial particles in turbulent boundary layers. Phys. Fluids 17, 098101.

Pirozzoli, S., Bernardini, M., Orlandi, P., 2011. Large-scale motions and inner/outer layer interactions in turbulent Couette–Poiseuille flows. J. Fluid Mech. 680, 534-563.

Reeks, M.W., 1983. The transport of discrete particles in inhomogeneous turbulence. J. Aerosol Sci. 14, 729–739.

Reeks, M.W., 2005. On model equations for particle dispersion in inhomogeneous turbulence. Intl J. Multiphase Flow 31, 93–114.

Reeks, M.W., 2014. Transport, mixing and agglomeration of particles in turbulent flows. Flow Turbul. Combust. 92, 3–25.

Richter, D.H., Sullivan, P.P., 2013. Momentum transfer in a turbulent, particle-laden Couette flow. Phys. Fluids 25, 053304.

Richter, D.H., Sullivan, P.P., 2014. Modification of near-wall coherent structures by inertial particles. Phys. Fluids 26, 103304.

Righetti, M., Romano, G.P., 2004. Particle–fluid interactions in a plane near-wall turbulent flow. J. Fluid Mech. 505, 93–121.

Rouson, D.W.I., Eaton, J.K., 2001. On the preferential concentration of solid particles in turbulent channel flow. J. Fluid Mech. 428, 149–169.

Schiller, L., Naumann, A.Z., 1933. Über die grundlegenden Berechnungen bei der Schwerkraftaufbereitung. Ver. Deut. Ing., 77, 318–320.

Schoppa, W., Hussain, F., 2002. Coherent structure generation in near-wall turbulence. J. Fluid Mech. 453, 57–108.

Skartlien, R., 2007. Kinetic modeling of particles in stratified flow−Evaluation of dispersion tensors in inhomogeneous turbulence. Intl J. Multiphase Flow 33, 1006–1022.

Soldati, A., Marchioli, C., 2009. Physics and modelling of turbulent particle deposition and entrainment: Review of a systematic study. Intl J. Multiphase Flow 35, 827–839.

Tennekes, H.T., Lumley, J.L., 1972. A first course in turbulence. The MIT Press.

Thurlow, E.M., Klewicki, J.C., 2000. Experimental study of turbulent Poiseuille–Couette flow. Phys. Fluids 12, 865–874.

Tsukahara, T., Kawamura, H., Shingai, K., 2006. DNS of turbulent Couette flow with emphasis on the large-scale structures in the core region. J. Turbul. 7, N19.

Yang, K., Zhao, L., Andersson, H.I., 2017. Turbulent Couette–Poiseuille flow with zero wall shear. Intl J. Heat Fluid Fl. 63, 14–27.

Zhao, L., Andersson, H.I., Gillissen, J.J.J. 2010. Turbulence modulation and drag reduction by spherical particles. Phys. Fluids 22, 081702.

Zhao, L.H., Marchioli, C., Andersson, H.I., 2012. Stokes number effects on particle slip velocity in wall-bounded turbulence and implications for dispersion models. Phys. Fluids 24, 021705.

Zhao, L., Andersson, H.I., Gillissen, J.J.J. 2013. Interphasial energy transfer and particle dissipation in particle-laden wall turbulence. J. Fluid Mech. 715, 32-59.